

EFFICIENT PART'S SHAPE AND ITS PLACEMENT IN CLOSED SPACE UNDER THERMAL ENERGY TREATMENT

Sergiy Plankovskyy¹, Yevgen Tsegelnyk¹, Olga Shypul², Tetyana Romanova^{3,4}, Volodymyr Kombarov^{1,5}

¹O.M. Beketov National University of Urban Economy in Kharkiv, Kharkiv, Ukraine

²National Aerospace University "Kharkiv Aviation Institute", Kharkiv, Ukraine

*³Anatolii Pidhornyi Institute of Power Machines and Systems
of the National Academy of Sciences of Ukraine, Kharkiv, Ukraine*

⁴University of Leeds, Leeds University Business School, Leeds, United Kingdom

*⁵Czech Technical University in Prague, Faculty of Mechanical Engineering,
Department of Production Machines and Equipment (RCMT), Prague, Czech Republic*

Email: y.tsegelnyk@kname.edu.ua

Abstract – The paper investigates an approach for optimizing the placement of complex-shaped parts during thermal energy treatment to ensure a uniform distribution of specific heat flux across the part's surface. The study demonstrates that the problem of sparsest packing can be addressed by aligning the centers of gravity and the principal central axes of inertia of thin shells, representing the outer surface of the part and the inner surface of the working chamber. For scenarios where complete alignment is unfeasible, the proposed method suggests determining the part's position by partially aligning selected principal axes of inertia and specific coordinates of the centers of gravity. The research advances the equivalent chamber method, enhancing modeling accuracy by reducing the principal central moments of inertia of the shell of an equivalent part. This is achieved using an inversely proportional relationship between its area and the area of the original part. The proposed approach proves effective in achieving uniform heating of complex-shaped parts during thermal energy treatment.

Keywords: Thermal Energy Treatment, Optimal Layout, Sparsest Packing, Heat Flow Distribution, Equivalent Part's Shape.

1. Introduction

The trend toward miniaturization in precision mechanisms has led to tighter tolerances in the friction and engagement pairs, necessitating higher accuracy in the parts that form them [1, 2]. As a result, edge finishing and surface cleaning technologies play a critical role in ensuring the reliability of these mechanisms. While abrasive techniques such as various flow abrasive processes [3, 4] and ultrasonic washing [5] have been widely used, they can lead to secondary contamination, especially in hydraulic and pneumatic components, where micro-abrasive particles can cause wear or jamming of friction pairs. This has spurred interest in deformation-free edge-finishing methods, such as electrochemical [6], electroerosive [7], and laser [8, 9] processing. However, these methods are complex, difficult to automate, and often require additional cleaning steps to remove residual particles.

The Thermal Energy Method (TEM) offers distinct advantages, particularly in the field of mechanical engineering for edge finishing [10, 11]. This method utilizes the energy produced by the combustion of lean gas mixtures. The parts to be processed

are placed in a sealed chamber filled with a fuel mixture. After combustion, the burrs formed during machining heat up and burn away when exposed to excess oxygen. Due to the significantly larger volume of the part compared to the burrs, the body of the part only experiences minimal heating (usually under one hundred degrees). The processing cycle duration in TEM equipment typically does not exceed two minutes. TEM outperforms other edge finishing methods in productivity, as it can simultaneously process multiple parts [12]. Since the combustion products come into contact with all surfaces of the parts at once, no additional mechanisms are needed to control the deburring process, offering significant opportunities for automation based on relatively simple CNC systems.

However, as noted in [13], the basic version of TEM does not allow for the simultaneous edge finishing and surface cleaning. Microparticles of abrasive materials, typically oxides, nitrides, or carbides of the metal, remain on the surface and cannot be removed by the combustion products of the fuel mixture. Additionally, due to prolonged contact with the hot oxygen-rich gas, the surfaces may develop an oxide layer. To remove these metal oxides, washing

[14] or pickling [15] is necessary. The Impulse Thermal Energy Method with Shock Waves (ITEMSW) generation represents a significant advancement in thermal processing techniques, specifically for deburring and cleaning precision parts. This method exploits the unique thermal characteristics of shock waves generated during the explosive combustion of fuel gas mixtures. Unlike TEM methods, which rely on steady combustion processes, ITEMSW utilizes a dynamic and highly controllable environment where the introduction of hot combustion gases can be precisely managed. This controlled supply of combustion products allows for a more flexible approach to thermal treatment, particularly for materials that are sensitive to overheating or have low melting points, such as thermoplastics [16]. A key feature of ITEMSW is its use of shock waves, which are created by the detonation or volumetric explosion of gas mixtures within the chamber. The rapid displacement of gases during these events leads to a dramatic increase in heat flux, with values that can exceed those observed during traditional deflagration combustion by factors of 10 to 100 [17]. This elevated heat transfer intensity is critical for enhancing the effectiveness of the thermal treatment process. The ability to rapidly transfer heat to parts allows for more efficient removal of burrs and other surface contaminants, making ITEMSW highly effective for precision cleaning and finishing applications. Additionally, ITEMSW's ability to generate localized, high-intensity heat fluxes makes it particularly useful in industries such as additive manufacturing (3D printing) [18], where complex-shaped parts often require cleaning from non-sintered powder particles without damaging the material [19].

Despite its advantages, ITEMSW faces challenges related to the non-uniformity of heat fluxes within the treatment chamber [20]. Due to the explosive nature of the shock waves, heat distribution across the chamber can be uneven, with certain areas receiving higher heat concentrations than others. This uneven distribution may lead to overheating of sensitive parts or inconsistent thermal effects, which can compromise the quality of the thermal treatment process. In some cases, this could even result in the deposition of metal oxides on part surfaces, potentially affecting the parts' performance or aesthetic quality. To mitigate these issues, it is essential to optimize the placement of parts within the chamber to achieve a more uniform distribution of heat. One effective strategy to address this is the concept of sparse packing, which involves positioning parts within the chamber as distantly as possible from each other [21, 22]. Sparse packing seeks to minimize the influence of thermal zones that could lead to overheating by reducing the proximity of adjacent parts. This technique is particularly valuable in situations where the thermal effects of the shock waves could result in excessive heat accumulation or thermal gradients across the parts. By ensuring that the

parts are spaced out appropriately, sparse packing can help reduce the likelihood of temperature discrepancies and improve the overall effectiveness of the thermal treatment process. The aim of the paper is to develop a method for optimizing the uniformity of heat fluxes during the ITEMSW by employing sparse packing techniques in the deburring chamber. This approach seeks to improve heat distribution, minimize overheating, and enhance the overall effectiveness of the thermal treatment process.

2. Part Optimal Layout Problem Formulation

To ensure stable quality during thermal energy treatment, it is crucial to maintain consistent processing conditions across all surfaces and edges. Since the primary factor influencing the outcome of thermal energy treatment is the heating of processed parts through contact with combustion products, stabilizing the treatment quality requires achieving uniform specific heat flux across the surfaces of the processed parts.

For thermal energy treatment under the influence of shock waves, the intensity of specific heat fluxes is determined by the frequency of their interaction with the processed parts. If the parts are not optimally arranged within the chamber, the specific heat fluxes acting on their surfaces can vary significantly (by several orders of magnitude) [20], making it impossible to achieve consistent quality in thermal energy treatment. Therefore, ensuring uniform processing conditions is a critical objective in the design of technological devices for thermal energy treatment.

In practice, when positioning individual parts with relatively simple shapes, they are typically placed near the axis of the working chamber. For group processing, they are arranged with cyclic symmetry around this axis [23]. However, these approaches are not suitable for processing non-symmetrical parts with complex shapes, such as those produced by 3D printing methods [18]. These parts often require additional machining to achieve the specified accuracy [24].

As noted in [20], during the development stage of a technological process for thermal energy treatment, the primary factor considered is the specific heat flux averaged over the surface of the processed part. To ensure consistent processing conditions when determining the position of parts during thermal energy treatment, it becomes essential to minimize the root mean square deviation of the specific heat flux on the surface from its mathematical expectation.

$$\sigma = \sqrt{\frac{\int_S (q - M(q))^2 dS}{\int_S dS}} \rightarrow \min, \quad (1)$$

where q is the value of the specific heat flow on the surface of the processed part with the surface S ; $M(q) = \int_S q dS / \int_S dS$ is a mathematical expectation of the specific heat flux.

The problem under consideration has not been addressed in any known studies related to thermal energy treatment. It significantly differs from the well-established issues associated with optimal layout. Consequently, solving this problem necessitates the development of novel approaches.

3. Sparsest Balancing Packing Problem

This problem was first formulated in [25] as the problem of the sparsest packing. As noted in the review [26], previously known optimal packing problems can be classified into the following categories:

- optimal cutting and minimization of undercuts;
- hopper packing, double packing, strip packing, and knapsack problems;
- loading problems, such as vehicles, pallets, and containers;
- separation, composition, nesting, and partitioning problems;
- capital budgeting, line balancing, memory allocation, and multi-processor scheduling problems.

The task of placing objects as densely as possible within a given area is typically addressed in such problems. In some cases, additional constraints are imposed on the solution. For example, in balanced layout problems, the placement must also account for requirements concerning the location of the center of mass of the objects. In thermal energy treatment methods, such as ITEMSW, the problem of locating the processed parts can be formulated as the task of positioning three-dimensional objects within the camera, ensuring uniform spacing between the objects and maintaining a consistent distance from the camera's surface. This hypothesis was introduced in paper [25]. This approach is motivated by the fact that, during the occurrence of shock waves following the detonation or thermal explosion of a fuel mixture, the heating of the processed parts' surfaces is influenced by the frequency of these waves. Furthermore, this frequency is determined by the distances between surfaces that reflect such waves.

Such problems can be categorized as optimal layout problems. Typically, when addressing these issues, three-dimensional objects are approximated by simpler geometric shapes for which well-established methods of optimal placement exist. To apply this approach, it is necessary to define a method for such approximations. To formulate the problem, consider the optimal placement of a material point o_1 within a specified domain Ω . As the criterion of optimality, the minimization of the expected value of the square

of the distance between o_1 and the boundary points of the domain Ω is proposed: $M(\|o_1 - o_\Omega\|^2) \rightarrow \min$.

In a two-dimensional formulation, this criterion can be expressed as:

$$M(\|o_1 - o_\Omega\|^2) = \int_{\Gamma_\Omega} \frac{(x_{o_\Omega} - x_{o_1})^2 + (y_{o_\Omega} - y_{o_1})^2}{L_\Omega} \Gamma_\Omega \rightarrow \min, \quad (2)$$

where Γ_Ω represents the curve forming the boundary of the placement area, and L_Ω denotes the length of the Γ_Ω curve.

If the axes OX and OY are chosen to pass through the center of gravity of the curve Γ_T , condition (2) can be rewritten as follows:

$$M(\|o_1 - o_\Omega\|^2) = \frac{J_x^\Omega + J_y^\Omega}{L_\Omega} + (x_{o_1}^2 + y_{o_1}^2) \rightarrow \min, \quad (3)$$

where J_x^Ω and J_y^Ω represent the axial moments of inertia of the Γ_Ω curve concerning the corresponding axis.

Considering that the sum of the axial moments of inertia of an arbitrary body with respect to axes passing through its center of gravity is a constant value, it follows from (3) that the minimum sought is achieved at $x_{o_1} = y_{o_1} \equiv 0$. This corresponds to the point located at the center of gravity of the curve that bounds the placement area.

Similarly, the same conclusion can be drawn for the problem of positioning two-dimensional or three-dimensional objects if we consider that their surfaces consist of a set of points. This result is not new and was first obtained in [27], where the ICP (Iterative Closest Point) algorithm was proposed for point cloud alignment problems, minimizing the sum of squared distances between the nearest points of the clouds. Various versions of the ICP algorithm have been developed in numerous studies, particularly in relation to virtual localization problems [28, 29]. However, the basic idea of the algorithm – superimposing the centers of mass of the combined point clouds at the first step – has been preserved in all versions. The disadvantage of such approaches is that they do not allow for the determination of the orientation of the placed object relative to the OX and OY axes. To address this shortcoming as an optimization criterion, the minimization of the difference between the squares of the radii of inertia of the curves defining the boundary of the area (Γ_Ω) and the placed object (Γ_T) relative to the principal central axes of inertia of the curve Γ_Ω can be used [25].

This approach, without losing generality, can be illustrated using the example of a two-dimensional problem. Suppose that the maximum principal central moment of inertia of the curve limiting the placement area J_{max}^Ω corresponds to the moment of

inertia about the OY axis, and the minimum J_{min}^{Ω} corresponds to the moment of inertia about the OX axis. To determine the optimal orientation of the object in relation to the placement area, we will require the following conditions:

$$r_{max\Omega}^2 - r_{yT}^2 = \frac{J_{max}^{\Omega}}{L_{\Omega}} - \frac{J_{max}^T \cos^2 \theta_1 + J_{min}^T \sin^2 \theta_1}{L_T} \rightarrow \min, \quad (4)$$

$$r_{min\Omega}^2 - r_{xT}^2 = \frac{J_{min}^{\Omega}}{L_{\Omega}} - \frac{J_{min}^T \cos^2 \theta_1 + J_{max}^T \sin^2 \theta_1}{L_T} \rightarrow \max, \quad (5)$$

where J_{min}^T and J_{max}^T are the principal central moments of inertia of the curve Γ_T , which defines the boundary of the object being placed.

Both criteria are satisfied when $\theta_1 = 0$, which results in the requirement for the coincidence of the main central axes of the curves Γ_T and Γ_{Ω} . Therefore

$$\min(r_{max\Omega}^2 - r_{yT}^2) = \frac{J_{max}^{\Omega}}{L_{\Omega}} - \frac{J_{max}^T}{L_T}, \quad (6)$$

$$\max(r_{min\Omega}^2 - r_{xT}^2) = \frac{J_{min}^{\Omega}}{L_{\Omega}} - \frac{J_{min}^T}{L_T}. \quad (7)$$

Expressions (6) and (7) can be used to solve two problems related to the development of thermal energy treatment technologies. First, they help determine the shape of equivalent parts when calculating surface-averaged specific heat fluxes. From a methodological perspective, this completes the formulation of the equivalent chamber method described in the previous chapter. Second, they assist in determining the positioning of the processed parts by replacing the original parts with geometric objects of a simple form, which are derived through operations with geometric primitives. In both cases, when the object T placed in the domain Ω is replaced by a body of simple form T_i , we will require the conditions: $\min(r_{max\Omega}^2 - r_{yT_i}^2) \rightarrow idem$ and $\max(r_{min\Omega}^2 - r_{xT_i}^2) \rightarrow idem$, which leads to the following dependences:

$$\frac{J_{min}^{T_i}}{L_{T_i}} = \frac{J_{min}^T}{L_T}, \quad \frac{J_{max}^{T_i}}{L_{T_i}} = \frac{J_{max}^T}{L_T}.$$

In the three-dimensional case, these conditions are formulated for thin shells that are stretched over the outer surface of the original part and the body it is replacing:

$$\frac{J_x^{T_i}}{S_{T_i}} = \frac{J_x^T}{S_T}, \quad \frac{J_y^{T_i}}{S_{T_i}} = \frac{J_y^T}{S_T}, \quad \frac{J_z^{T_i}}{S_{T_i}} = \frac{J_z^T}{S_T}, \quad (8)$$

where OX , OY , and OZ are the principal central axes of the shells of bodies T and T_i , and S_T and S_{T_i} are the areas of their external surfaces.

Let's proceed with formulating the problem of the sparsest balanced packing to determine the optimal placement of parts during thermal energy treatment. For simplicity in explanation, we will consider the problem in a two-dimensional formulation. We consider the set of objects $T_i \subset R^2$, where $i \in I_n = \{1, \dots, n\}$, placed in the container Ω . We assume that each object T_i , for $i \in I_n$, can be represented as $T_i = \bigcup_{s=1}^{n_i} T_{is}$, where T_{is} is either a circle or a polygon. This choice of object forms does not limit the generality of the problem, as any arbitrary object T can be reduced to the form $T_i = \bigcup_{s=1}^{n_i} T_{is}$ as described above [21].

Each circle is defined by its radius, and each polygon is defined by its vertices in the local coordinate system associated with the object T_i . The problem at hand involves optimally positioning objects T_i , where $i \in I_n$, and allowing them to move and rotate continuously. We define the motion vector of object T_i as $\mathbf{u}_i = (\mathbf{v}_i, \theta_i)$, where $\mathbf{v}_i = (x_i, y_i)$ is the translation vector, and θ_i is the angle of rotation, for $i \in I_n$. The center of gravity of the curve Γ_{T_i} , which is the boundary of the object T_i , coincides with the origin of its local coordinate system. The rotation of object T_i by angle θ_i and translation along vector \mathbf{v}_i is defined as

$T_i(\mathbf{u}_i) = \{p \in R^2 : p = \mathbf{v}_i + \Xi(\theta_i) \cdot (p^0)^T, \forall p^0 \in T_i^0\}$, where T_i^0 is the original, untransformed object, and $\Xi(\theta_i)$ is the rotation matrix corresponding to angle θ_i :

$$\Xi(\theta_i) = \begin{pmatrix} \cos \theta_i & \sin \theta_i \\ -\sin \theta_i & \cos \theta_i \end{pmatrix}.$$

The vector $\mathbf{u}_i = (\mathbf{v}_i, \theta_i)$ determines the location of objects T_i , where $i \in I_n$, in the Euclidean space R^2 . Here, $\mathbf{v} = (v_1, \dots, v_n)$ and $\theta = (\theta_1, \dots, \theta_n)$. The curve Γ_{T_i} , which defines the boundary of each object T_i , has a weight determined by its length L_i , where $i \in I_n$. The weight of the boundary curve Γ_{Ω} , which defines the boundary of the container Ω , is denoted by L_{Ω} . We assume that, in the coordinate system of the container, with the main central axis of inertia of the curve Γ_{Ω} , the center of gravity of each object $T_i(\mathbf{u}_i)$ located at the point \mathbf{v}_i coinciding with the origin of its local coordinate system. Therefore, the center of gravity $\mathbf{v} = (x_c, y_c)$ of the system of objects placed inside the container is determined as:

$$x_c(\mathbf{v}) = \sum_{i=1}^n \frac{L_i}{L} x_i, \quad y_c(\mathbf{v}) = \sum_{i=1}^n \frac{L_i}{L} y_i, \quad (9)$$

where $L = \sum_{i=1}^n L_i$.

We will require that the deviation of the center of gravity $\mathbf{v} = (x_c, y_c)$ from the origin $(0,0)$ be within the following limits:

$$|x_c| \leq \delta, \quad |y_c| \leq \delta, \quad (10)$$

where $\delta > 0$ is the specified positioning error.

Assume that

$$dist(T_i(u_i), T_j(u_j)) = \min_{t_i \in \Gamma_{T_i(u_i)}, t_j \in \Gamma_{T_j(u_j)}} \|t_i - t_j\|$$

represents the Euclidean distance between $T_i(u_i)$ and $T_j(u_j)$, and $dist(T_i(u_i), \Omega) = \min_{t_i \in \Gamma_{T_i(u_i)}, t \in \Gamma_{\Omega}} \|t_i - t\|$

is the distance between the object $T_i(u_i)$ and the container Ω . The packing of objects T_i inside the container Ω will be considered the most sparse if it maximizes the minimum distance between each pair of objects T_i and T_j , as well as the distance between each object T_i and the container Ω , i.e.,

$$\min \left\{ \begin{array}{l} dist(T_i(u_i), T_j(u_j)) > 0, \\ i < j = 1, \dots, n; \\ dist(T_i(u_i), \Omega) > 0, \\ i = 1, \dots, n. \end{array} \right\} \rightarrow \max. \quad (11)$$

The problem of balanced sparsest packing involves determining the sparsest arrangement of objects T_i , $i \in I_n$ under the condition described in (11), while also taking into account the balancing conditions outlined in (10). In the three-dimensional case, the problem of the sparsest balanced packing is formulated similarly. However, in this case, the expressions of type (9) do not include the lengths of the curves, but rather the areas of thin shells stretched between the objects T_i and the inner surface of the container Ω . In accordance with the conditions in (10), a constraint is added for the coordinate z_c . We now consider how the formulated problem can be applied to derive the method of the equivalent chamber.

3. Numerical Experiment

The verification of the hypotheses formulated in the previous section was carried out through a numerical experiment. The primary objective was to estimate the error in determining the values of the specific heat flux averaged over the surfaces of objects with sufficiently complex shapes when an equivalent part replaces them. The experiment was conducted under the following conditions: (i) the centers of gravity of the thin shells stretched over the surfaces of both the original and equivalent parts are identical; (ii) the main central axes of inertia of the thin shells stretched over the surfaces of the original and equivalent parts coincide; (iii) condition (8) holds for both the original and equivalent parts.

In the course of numerical experiments, heating under shock wave conditions was simulated. For this

purpose, a heat exchange problem in a chamber filled with gas at a specified temperature and pressure was considered. The calculation scheme for the test problem is shown in Fig. 1. The combustion of gases was modeled based on a set of equations that describe the conservation of mass, momentum, energy, and species. These equations, excluding mass forces, baro-diffusion, and thermal diffusion, are detailed in [30].

The SAS SST turbulence model was employed for the calculations [31]. Kader's solution was applied [32] to determine the convective heat flux. For the combustion simulation, the Premixed FGM (Flamelet-Generated Manifold) model was utilized in Reaction Progress Variable Space. This model solves a transport equation for the mean reaction progress variable, which is defined as a normalized sum of the product species mass fractions. The equations governing premixed flames can be transformed from physical space to reaction progress space, assuming negligible differential diffusion [33, 34]. In this study, the combustion process was simulated using hydrogen as the fuel gas and air as the oxidant. The numerical simulations were performed with the commercial software ANSYS Fluent. The chemical reactions were modeled using the GRI-Mech 3.0 mechanism with thermodynamic properties of all species expressed as fourth-degree polynomial functions [35].

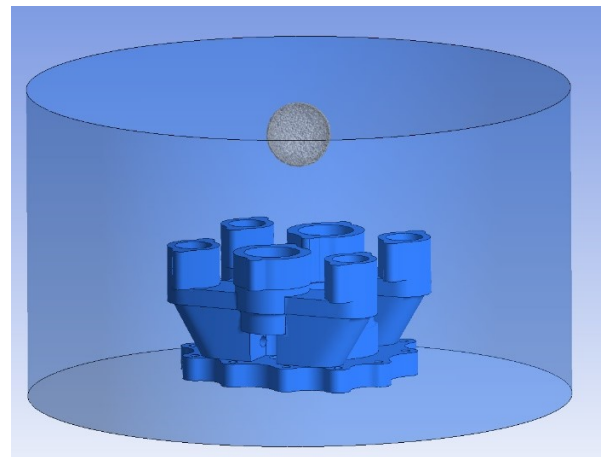


Figure 1: Schematic diagram for calculating the specific heat fluxes in a spherical high-pressure zone

The computational grid near the walls was constructed in accordance with the y^+ spacing recommendations for the SST turbulence model. The simulations were conducted using transient analysis to capture the time-dependent behavior. To address the high gradients of pressure and velocity, a time step of 10^{-5} seconds was employed with the pressure-based solver. A summary of the solver parameters used in this study is provided in Table 1.

Table 1: Summary of solver parameters

Parameter	Value
Solver	Pressure-based (segregated)
Pressure -Velocity coupling	COUPLED
Spatial discretization	Second-order/second-order UPWIND
Temporal discretization	Second-order implicit
Gradient discretization	Least-squares cell-based

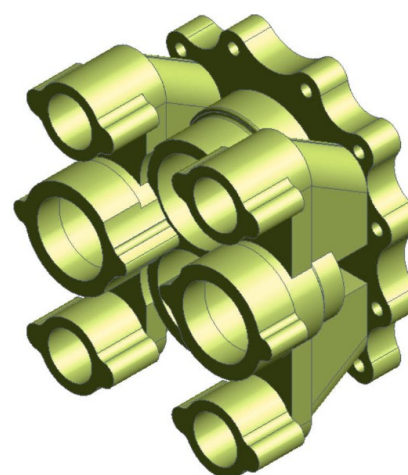
The original and equivalent parts were placed in the chamber where conditions (i) and (ii) were satisfied. The chamber was assumed to be filled with gas at pressure P_0 and temperature T_0 . In this way, the conditions for a thermal explosion of a portion of the fuel mixture were simulated, which represents one of the regimes in the thermal energy treatment of metal parts. In the middle of the chamber, for both cases, a region of increased pressure $P = P_0 + \Delta P$ was created in the form of a spherical region with the same diameter. The problem of shock wave propagation and attenuation was then solved.

The condition for stopping the simulation was specified by the expression $\max(P)/\min(P) \leq 1.05$. The time when this condition was satisfied was considered the time of shock wave attenuation. During the simulation, the specific heat fluxes on the surfaces of the parts were determined.

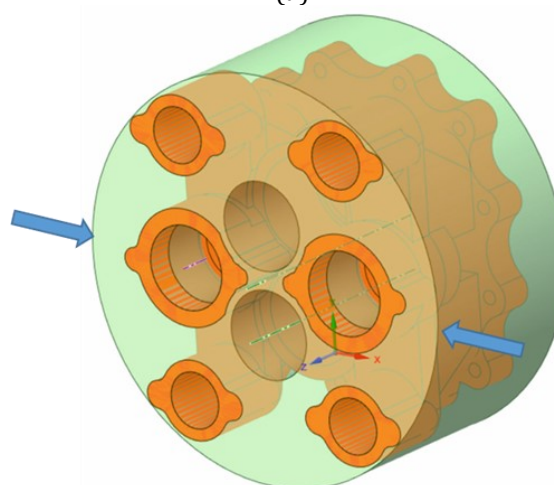
The temperature of the part walls was kept constant, and the chamber wall was treated as adiabatic. This formulation was chosen because the aim of the calculations was not to determine the exact values of the specific heat fluxes, which would require considering the heat losses of the combustion products in heating the chamber walls. Instead, the focus was on evaluating the errors caused by replacing the original part with an equivalent one, as well as the related computational resource requirements.

Two variants of constructing an equivalent part were considered. In the first, taking into account the symmetry of the original part, it was constructed as follows.

1. The part was fitted into a cylinder with a height equal to the height of the original part (Fig. 2). Then, the resulting cylinder was compressed by scaling along the OX axis so that the ratio of the principal central moments of inertia of the thin shell stretched over its surface matched the corresponding ratio for the original part:



(a)



(b)

Figure 2: Creating an equivalent part from a geometric primitive: (a) Original part; (b) Stage of constructing the equivalent part

$$\left. \begin{aligned} \frac{J_x^{eq}}{J_y^{eq}} &= \frac{J_x^p}{J_y^p} \\ \frac{J_x^{eq}}{J_z^{eq}} &= \frac{J_x^p}{J_z^p} \end{aligned} \right\} \quad (12)$$

where $J_x^{eq}, J_y^{eq}, J_z^{eq}$ are the principal central moments of inertia of the thin shell stretched over the outer surfaces of the equivalent part, and J_x^p, J_y^p, J_z^p are the corresponding moments for the original part.

The shape of the geometric primitive into which the original detail will fit should be selected based on its shape. Depending on the specific case, it can be a cylinder, parallelepiped, prism, or other appropriate form.

2. In the second step, the equivalent part is scaled along all coordinates to satisfy the conditions in (8). Specifically, taking into account the notations introduced in (12), the following conditions must be fulfilled:

$$\frac{J_x^{eq}}{S_{eq}} = \frac{J_x^p}{S_p}, \quad \frac{J_y^{eq}}{S_{eq}} = \frac{J_y^p}{S_p}, \quad \frac{J_z^{eq}}{S_{eq}} = \frac{J_z^p}{S_p},$$

for this, the geometric primitive modified in the previous step is scaled by the factor $k = \sqrt{S_{eq}/S_p}$.

3. If the original part contains developed holes or internal cavities, similar steps are taken to create an equivalent part for the internal volume of the original. For this purpose, it is useful to employ filling tools, which are available in most CAD systems, including the geometric modules of ANSYS Design Modeler and SpaceClaim. The final shape of the equivalent part is obtained by performing a Boolean subtraction of the equivalent part for the internal volume from the equivalent part for the outer shape.

Figure 3 shows the results of the calculation of the average specific heat flow over the surface of both the original and equivalent parts (for the case shown in Fig. 1) during shock wave damping. The specific heat flux estimates the error averaged over the surface and the processing time

$$\delta = \frac{\left| \frac{1}{\tau_y^p} \int_0^{\tau_y^p} \left(\frac{J_{sp} q dS}{S_p} \right) dt - \frac{1}{\tau_y^{eq}} \int_0^{\tau_y^{eq}} \left(\frac{J_{seq} q dS}{S_{eq}} \right) dt \right|}{\frac{1}{\tau_y^p} \int_0^{\tau_y^p} \left(\frac{J_{sp} q dS}{S_p} \right) dt} \times 100\%, \quad (13)$$

where τ_y^p and τ_y^{eq} represent the shock wave damping times for the original and equivalent parts, respectively.

For the case under consideration, the calculation error according to expression (13), caused by the transition from the original part to the equivalent part, does not exceed 2.5%. Furthermore, the time required to obtain a solution with the same calculation grid parameters was 2.5 hours for the original part and 0.5 hours for the equivalent part, which is five times shorter.

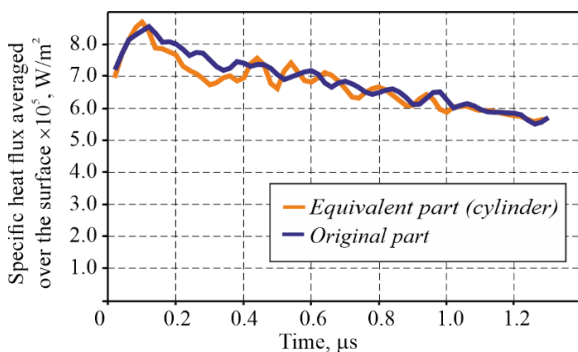


Figure 3: Results of specific heat flow calculations for the original and equivalent parts

When the shape of the part to be processed is too complex to fit into a geometric primitive, an alternative approach can be used to construct an equivalent part for calculating the averaged specific heat fluxes. This approach involves creating the shape of an

equivalent part through Boolean operations with several geometric primitives.

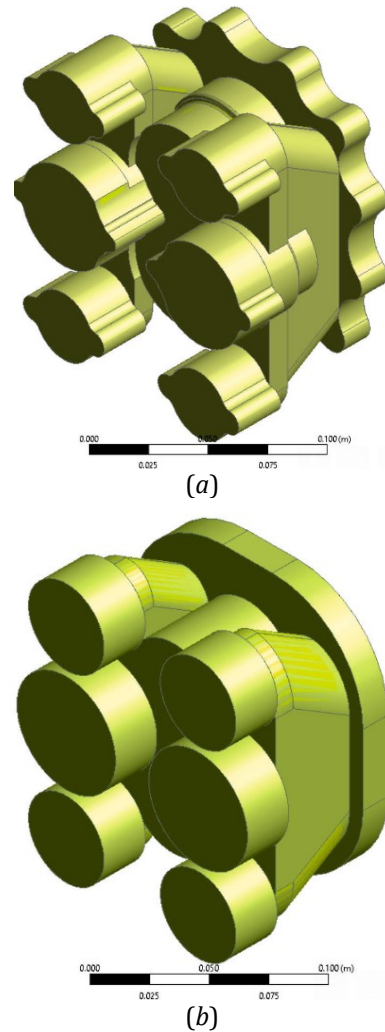


Figure 4: Creating an equivalent part using several primitive shapes

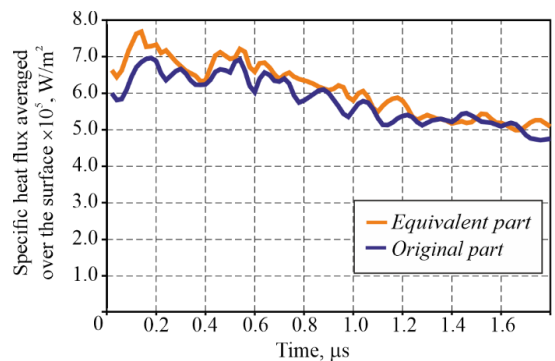


Figure 5: Results of specific heat flow calculations for the original and equivalent parts

As an example, consider the sequence of constructing such an equivalent part for the detail previously discussed. The simplest method is to remove certain components from the 3D model construction tree of the original part within the CAD module project. The sequence for building the equivalent part in this case is as follows.

As in the previous case, a standard CAD tool from the 'filling' type systems (Fig. 4, a) is used to fill the internal cavities of the original part (Fig. 2, a). Afterward, the links responsible for constructing the small elements are removed from the project tree, and the equivalent part is built using the minimum number of geometric primitives (Fig. 4, b).

Subsequently, steps 2 and 3, as described above for the case of an equivalent part derived from a modified geometric primitive, are carried out to construct the equivalent part.

Figure 5 shows the results of calculating the surface-averaged specific heat flux of the original and equivalent parts during shock wave attenuation. The error, calculated according to expression (13) for the considered case, was 5%. At the same time, the time required to obtain a solution with the same grid parameter settings for the equivalent part was 1 hour, which is 2.5 times less than the time required for calculations of the original part.

4. Balanced Packing of 3D Objects Considering the Impact of Shock Waves

In a subsequent group of numerical experiments, conclusions regarding the optimal conditions for the placement of objects were validated. Specifically, the alignment of the centers of gravity and the main central axes of inertia for thin shells stretched over the inner surface of the working chamber and the surface of the placed object were examined. The mathematical model used for the numerical experiments includes a system of defining equations described in [30]. The original and equivalent parts were placed in the chamber with conditions (i) and (ii) satisfied. The chamber was assumed to be filled with gas at a specified pressure and temperature. In the corner of the chamber, for all calculated cases, an area of increased pressure was modeled as a quarter of a torus with the same diameter. The problem of shock wave propagation and attenuation was then solved. As in the previously discussed cases, the stopping condition for the calculation was defined by the expression $\max(P)/\min(P) \leq 1.05$. During the simulation, specific heat flows on the surfaces of the parts were determined. The temperature of the part walls was set as constant, while the chamber wall was considered adiabatic. The objective of the simulation was to confirm the conclusions that the optimal configuration, in terms of the uniform distribution of specific heat fluxes on the chamber surface under the impact of shock waves, occurs when the centers of gravity and the main central axes of inertia of the thin shells, stretched over the surface of the processed part and the inner surface of the chamber, are aligned.

To verify this, three cases were considered: the part is positioned in the chamber according to the formulated requirements (Fig. 6, a); the part is shift-

ed relative to the optimal position (Fig. 6, b); and the part is rotated relative to the optimal position (Fig. 6, c).

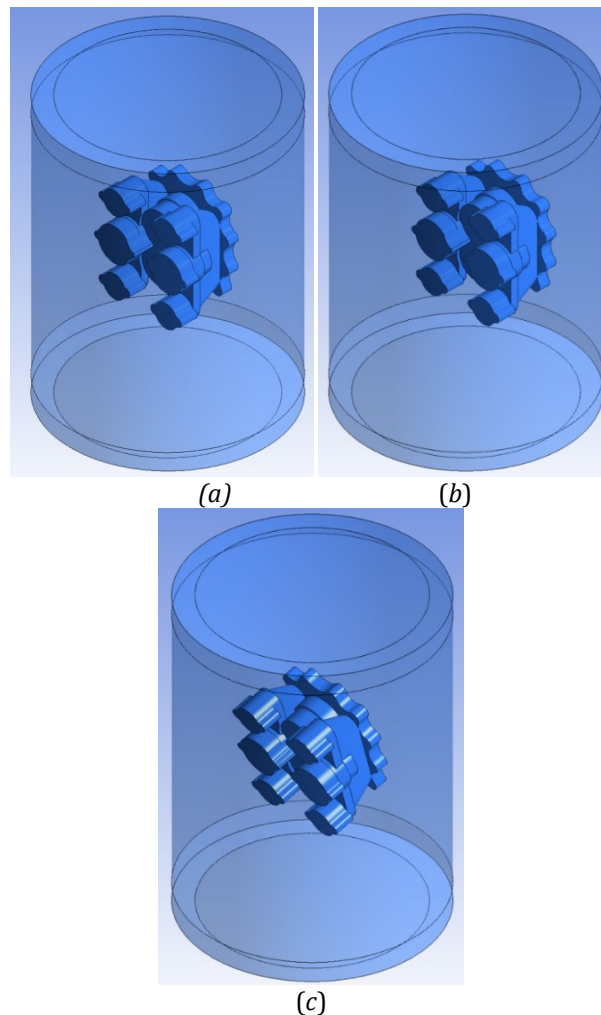


Figure 6: Calculation schemes for determining the optimal layout of parts based on the uniformity of specific heat flow distribution

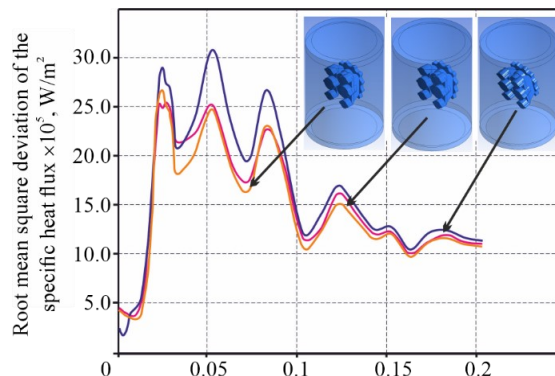


Figure 7: Results of the evaluation of the uniformity of heat flow distribution under different part positioning conditions in the chamber

Figure 7 presents the results of estimating the specific heat flux averaged over the surface of the parts during shock wave attenuation. The optimality

of the layout was assessed based on the condition of minimizing the root-mean-square deviation of the surface-averaged specific heat flux (1). As shown in the dependencies in Figure 7, calculated using Eq. (1) for the cases considered, the maximum deviation of the surface-averaged specific heat flux during the entire shock wave attenuation process occurred for the configuration where the centers of gravity and the principal central axes of inertia of the thin shells, stretched over the part's surface and the inner surface of the chamber, coincided. This configuration was found to be optimal.

Thus, the described technique extends the equivalent chamber method presented in [20] and enables the calculation of the energy parameters of thermal energy treatment (including the averaged specific heat flux and shock wave decay time) with a significant reduction in computational costs.

5. Conclusions

The paper demonstrates that the problem of determining the position of a part with a complex shape during thermal energy treatment can be addressed by combining the centers of gravity and the principal central axes of inertia of thin shells. These axes coincide with the outer surface of the part and the inner surface of the working chamber. The example test cases show that this arrangement is optimal for ensuring a uniform distribution of specific heat flux over the surface of the processed part. If such an alignment is not possible, the position of the processed part must be determined by aligning the principal central axes and the coordinates of the centers of gravity individually.

The equivalent chamber method, proposed in [20] for thermal energy treatment of complex-shaped parts, has been further developed. Unlike previous approaches, it is demonstrated that to apply this method, alignment of the centers of gravity and the principal central axes of inertia of thin shells – coinciding with the surfaces of the original and equivalent parts – is necessary. The dimensions of the equivalent part are determined by minimizing the central moments of inertia of the shells relative to the central moments of inertia of the original part, using an inversely proportional ratio of their areas.

Acknowledgement

The research was supported by the European Union Assistance Instrument for the Fulfilment of Ukraine's Commitments under the Horizon 2020 Framework Program for Research and Innovation (Research Project No. 0124U004371), partially by the EURIZON project (Grant Agreement No. 871072), and by the British Academy (Grant No. 100072).

References

- [1] Schellekens, P., Rosielle, N., Vermeulen, H., Vermeulen, M., Wetzels, S., & Pril, W. (1998). Design for precision: current status and trends. *CIRP Annals*, 47(2), 557–586.
- [2] Dobrotvorskiy, S., Basova, Y., Ivanova, M., Kotliar, A., & Dobrovolska, L. (2018). Forecasting of the productivity of parts machining by highspeed milling with the method of half-overlap. *Diagnostyka*, 19(3), 37–42.
- [3] Petare, A.C., & Jain, N.K. (2018). A critical review of past research and advances in abrasive flow finishing process. *The International Journal of Advanced Manufacturing Technology*, 97, 741–782.
- [4] Dolmatov, A.I., Sergeev, S.V., Kurin, M.O., Voronko, V.V., & Loza, T.V. (2015). Kinematics of the solid particle accelerated by a flow of gas in a supersonic nozzle and work hardening of the processed surface. *Metallofizika i Noveishie Tekhnologii*, 37(7), 871–885.
- [5] Yamashita, T., Yamauchi, R., & Ando, K. (2018). Progress in ultrasonic cleaning research. *Japanese Journal of Multiphase Flow*, 32(2), 210–217.
- [6] Kadam, S.P., & Mitra, S. (2021). Electrochemical deburring-A comprehensive review. *Materials Today: Proceedings*, 46, 141–148.
- [7] Jeong, Y.H., HanYoo, B., Lee, H.U., Min, B.K., Cho, D.W., & Lee, S.J. (2009). Deburring microfeatures using micro-EDM. *Journal of Materials Processing Technology*, 209(14), 5399–5406.
- [8] Song, H., & Wu, B. (2022). Physics-based modeling and micro-burr removal mechanism analysis for laser-induced plasma deburring. *Journal of Manufacturing Processes*, 75, 1217–1229.
- [9] Bernatskyi, A., Sydorets, V., Berdnikova, O.M., Krivtsun, I., & Chinakhov, D.A. (2020). Pore formation during laser welding in different spatial positions. *Solid State Phenomena*, 303, 47–58.
- [10] Lamikiz, A., Ukar, E., Tabernerero, I., & Martinez, S. (2011). Thermal advanced machining processes. In J.P. Davim (Eds.), *Modern Machining Technology* (pp. 335–372). Woodhead Publishing.
- [11] Benedict, G.F. (2017). Thermal energy method: deburring (TEM). In *Nontraditional Manufacturing Processes* (pp. 349–361). CRC Press.
- [12] Gillespie, L.K. (1999). *Deburring and Edge Finishing Handbook*. Society of Manufacturing Engineers.
- [13] Plankovskyy, S., Popov, V., Shypul, O., Tsegelnyk, Y., Tryfonov, O., Brega, D. (2021). Advanced thermal energy method for finishing precision parts. In K. Gupta & A. Pramanik (Eds.), *Advanced Machining and Finishing* (pp. 527–575). Elsevier.
- [14] Lutz, T. (2019). Oxide nach thermischem Entgraten effektiv entfernen. *JOT Journal für Oberflächentechnik*, 59(9), 102–104.
- [15] Treptow, F., & Wulfestieg, K.P. (2017). Gentle removal of oxide layers. *IST International Surface Technology*, 10(3), 50–53.

- [16] Plankovskyy, S., Shypul, O., Tsegelnyk, Y., Brega, D., Tryfonov, O., & Malashenko, V. (2022). Basic principles for thermoplastic parts finishing with Impulse Thermal Energy Method. In K. Kumar, B. Babu, & J. Davim (Eds.), *Handbook of Research on Advancements in the Processing, Characterization, and Application of Lightweight Materials* (pp. 49–87). IGI Global.
- [17] Plankovskyy, S., Shypul, O., Tsegelnyk, Y., Pankratov, A., & Romanova, T. (2021). Amplification of heat transfer by shock waves for Thermal Energy Method. In M. Nechyporuk, V. Pavlikov, & D. Kritskiy (Eds.), *Integrated Computer Technologies in Mechanical Engineering – 2020*. LNNS, vol. 188 (pp. 577–587). Springer.
- [18] Vambol, O., Kondratiev, A., Purhina, S., & Shevtsova, M. Determining the parameters for a 3d-printing process using the fused deposition modeling in order to manufacture an article with the required structural parameters. *Eastern-European Journal of Enterprise Technologies*, 2(1), 70–80.
- [19] Sibanda, P.S., Carr, P., Ryan, M., & Bigot, S. (2019). State of the art in surface finish of metal additive manufactured parts. In Y. Jin, & M. Price (Eds.), *Advances in Transdisciplinary Engineering: Vol. 9. Advances in Manufacturing Technology XXXIII* (pp. 221–225). IOS Press.
- [20] Plankovskyy, S., Teodorczyk, A., Shypul, O., Tryfonov, O., & Brega, D. (2019). Determination of detonable gas mixture heat fluxes at thermal deburring. *Acta Polytechnica*, 59(2), 162–169.
- [21] Romanova, T., Pankratov, A., Litvinchev, I., Plankovskyy, S., Tsegelnyk, Y., & Shypul, O. (2021). Sparsest packing of two-dimensional objects. *International Journal of Production Research*, 59(13), 3900–3915.
- [22] Romanova, T., Stoyan, Y., Pankratov, A., Litvinchev, I., Plankovskyy, S., Tsegelnyk, Y., & Shypul, O. (2021). Sparsest balanced packing of irregular 3D objects in a cylindrical container. *European Journal of Operational Research*, 291(1), 84–100.
- [23] Struckmann, J., & Kieser, A. (2020). *Thermal Deburring*. ATL Anlagentechnik Luhden GmbH
- [24] Tsegelnyk, Y., Kombarov, V., Plankovskyy, S., Aksonov, Y., Pliuhin, V., & Aksonov, O. (2022). Investigation of the portal-type machine tool gearbelt gearbox. *International Journal of Mechatronics and Applied Mechanics*, 2022(11), 295–302.
- [25] Plankovskyy, S., Nikolaev, A., Shypul, O., Litvinchev, I., Pankratov, A., & Romanova, T. (2020). Balance layout problem with the optimized distances between objects. In P. Vasant, I. Litvinchev, J. A. Marmolejo-Saucedo, R. Rodriguez, & F. Martinez (Eds.), *Data Analysis and Optimization for Engineering and Computing Problems*. EAISICC (pp. 85–93). Springer.
- [26] Guo, B., Zhang, Y., Hu, J., Li, J., Wu, F., Peng, Q., & Zhang, Q. (2022). Two-dimensional irregular packing problems: A review. *Frontiers in Mechanical Engineering*, 8, 966691.
- [27] Besl, P.J., & McKay, N.D. (1992). Method for registration of 3-D shapes. In *Sensor Fusion IV: Control Paradigms and Data Structures* (Vol. 1611, pp. 586–606). SPIE.
- [28] Mehrad, V., Xue, D., & Gu, P. (2014). Robust localization to align measured points on the manufactured surface with design surface for freeform surface inspection. *Computer-Aided Design*, 53, 90–103.
- [29] Plankovskyy, S., Tsegelnyk, Y., Romanova, T., Pankratov, O., Litvinchev, I., & Kombarov, V. (2023). Using the phi-function technique for the optimized virtual localization problem. In P. Vasant, et al. (Eds.), *Intelligent Computing and Optimization*. LNNS, vol. 855 (pp. 277–287). Springer.
- [30] Plankovskyy, S., Romanova, T., Pankratov, A., Litvinchev, I., Tsegelnyk, Y., Shypul, O., & Vasant, P. (2023). Sparse 2D packing in thermal deburring with shock waves acting effects. In M.S. Manshahia, et al. (Eds.), *Human-Assisted Intelligent Computing: Modeling, simulations and applications* (pp. 13–1). IOP Publishing.
- [31] Menter, F.R. (1994). Two-equation eddy-viscosity turbulence models for engineering applications. *AIAA Journal*, 32(8), 1598–1605.
- [32] Kader, B.A. (1981). Temperature and concentration profiles in fully turbulent boundary layers. *International Journal of Heat and Mass Transfer*, 24(9), 1541–1544.
- [33] Nguyen, P.D., Vervisch, L., Subramanian, V., & Domingo, P. (2010). Multidimensional flamelet-generated manifolds for partially premixed combustion. *Combustion and Flame*, 157(1), 43–61.
- [34] Lodier, G., Vervisch, L., Moureau, V., & Domingo, P. (2011). Composition-space premixed flamelet solution with differential diffusion for in situ flamelet-generated manifolds. *Combustion and Flame*, 158(10), 2009–2016.
- [35] Marzouk, O. (2023). Adiabatic flame temperatures for oxy-methane, oxy-hydrogen, air-methane, and air-hydrogen stoichiometric combustion using the NASA CEARUN tool, GRI-Mech 3.0 reaction mechanism, and cantera Python package. *Engineering, Technology & Applied Science Research*, 13(4), 11437–11444.